Fourth order correlations in dynamic light scattering from flexible polymer chains: agreement of scaling laws with numerical predictions

William G. Griffin* and Mary C. A. Griffin
AFRC Institute of Food Research, Reading Laboratory, Shinfield, Reading, Berks, RG2 9AT, UK
(Received 13 January 1989; accepted 31 March 1989)

We present calculations of $g^{(2)}(\mathbf{k}_1, \mathbf{k}_2; t)$, the fourth order correlation function of the electric field amplitude of light scattered by a flexible polymer chain, with and without hydrodynamic interactions using the Rouse and Zimm models respectively. Calculations of the second order correlation function, $g^{(1)}(\mathbf{k}, t)$ are also presented. The results are shown to be in excellent agreement with theoretical scaling predictions in the limit of large N, N being the number of subunits in the chain. Calculations made using the Hearst approximation of the Zimm model show that numerical values of the scaling indices and the initial slopes of $g^{(1)}$ and $g^{(2)}$ undergo a smooth transition from the free-draining to the non-free draining limiting values as the strength of the hydrodynamic interaction is increased.

(Keywords: polymer; light scattering; photon cross-correlation spectroscopy; Rouse; Zimm; Oseen tensor)

INTRODUCTION

The technique of photon cross-correlation spectroscopy (PCCS) has been used previously to investigate the fourth order correlation function, $g^{(2)}(\mathbf{k}_1, \mathbf{k}_2; t)$ of ordered colloidal systems and dilute polymer solutions[1–4], where $\mathbf{k}_1$ and $\mathbf{k}_2$ are the scattering vectors corresponding to the positions of two detectors. In a recent publication[5] a theoretical framework was presented for computing $g^{(2)}$ for polymer chains of variable chain rigidity in the absence of hydrodynamic interactions using the Rouse[6] and Harris–Hearst[7] models to describe the internal dynamics of the chain. As is now well established[8], for long polymer chains in dilute solutions, hydrodynamic interactions have a significant effect on chain dynamics and self diffusion, so that a complete theoretical description of the wave vector dependence of $g^{(2)}$ must take these effects into account. In the present work, therefore, we compute $g^{(2)}$ and the initial decay rate, $\Gamma(\mathbf{k}_1, \mathbf{k}_2)$ for a Rouse–Zimm model of a polymer chain in dilute solution. In this model hydrodynamic interactions within a single chain are taken into account by means of a pre-averaged Oseen tensor[9]. The primary objective of this work is to establish, by numerical evaluation of the appropriate theoretical expressions, the dependence of $\Gamma(\mathbf{k}_1, \mathbf{k}_2)$ on kR_g, where R_g is the radius of gyration of the isolated polymer chain in dilute solution, and the variation of this dependence with N, the number of segments used in the model of the chain. We compare our findings with predictions based on scaling theory[10] and analytical calculations[11]. In view of the difficulty of solving analytically[12] more complex problems involving polymer dynamics in concentrated solutions and melts it is clearly desirable to have effective simulation and numerical analysis techniques available. However, limitations of computing speed and memory have necessitated, for concentrated polymeric systems, the use of rather small values for N. (For example, Baumgärtner and Binder[13] simulated an ensemble of interacting polymer chains each with $N = 16$ using a Monte Carlo technique. In a more recent study, Kolinski *et al.*[14–17] fail to reach the reptation regime in a model melt, using a lattice Monte Carlo simulation, even where N achieves values of 800.) In another context, Weill and des Cloiseaux[18] discussed the N dependence of static and dynamic properties of an isolated polymer chain in solution in an attempt to understand discrepancies between dynamical scaling law predictions and experiment. They observed, on the basis of a simple theoretical model for chain dynamics, that the dynamical properties of chains of N links converge much more slowly to the $N \to \infty$ asymptotes than the static properties. Caution is therefore needed in making generalizations on the basis of numerical calculations of chain dynamics. In this paper we present the N-dependence of dynamical properties of Rouse and Rouse–Zimm chains as reflected in the kR_g dependence of $g^{(1)}$ and $g^{(2)}$ for values of N sufficient to display the transition from subunit dynamics to an asymptote, which approaches closely the scaling law predictions. (Pusey[4] has shown how scaling law forms for the dependence of $g^{(2)}$ on kR_g can be obtained on the basis of an assumed power dependence of $g^{(1)}$ on kR_g for large values of kR_g.) Such numerical predictions for the kR_g dependence of $g^{(2)}$ will apply to the experimental situation where cross-correlation dynamic light scattering is carried out on very long flexible polymer chains in dilute, theta solution.

THEORY

For a detailed review of dynamic light scattering theory with the emphasis on the measurement of statistical properties of scattered light the review of Pusey[19] is

* To whom correspondence should be addressed

0032-3861/90/010024-09$03.00
© 1990 Butterworth & Co. (Publishers) Ltd.

recommended. What follows is intended to define our notation and describe briefly the theoretical models of polymer dynamics we have adopted. In a conventional, single-detector, dynamic light-scattering experiment the time-dependent electric field correlation function, $g^{(1)}(\mathbf{k}, t)$, is obtained from the measured intensity autocorrelation function. $g^{(1)}(\mathbf{k}, t)$ is given by[20]:

$$g^{(1)}(\mathbf{k}, t)=\frac{\langle E(\mathbf{k}, 0)E^*(\mathbf{k}, t)\rangle}{\langle I(\mathbf{k})\rangle} \tag{1}$$

where $E(\mathbf{k}, t)$ is the scattered field amplitude at time t, $I(\mathbf{k})$ is the mean scattered intensity and $\mathbf{k}$ is the scattering vector. If two detectors are set up to receive the light scattered by particles diffusing through the same small scattering volume and their outputs are cross-correlated we obtain the intensity cross-correlation function, $g^{(2)}(\mathbf{k}_1, \mathbf{k}_2; t)$, which is given by[1,4,5]:

$$g^{(2)}(\mathbf{k}_1, \mathbf{k}_2; t)=\frac{\langle I(\mathbf{k}_1, 0)I(\mathbf{k}_2, t)\rangle}{\langle I(\mathbf{k}_1)\rangle\langle I(\mathbf{k}_2)\rangle} \tag{2}$$

$$=\begin{cases} 1+\beta|g^{(1)}_{\mathrm{INT}}(\mathbf{k}, t)|^2+g^{(2)}_{\mathrm{NG}}(\mathbf{k}, t) & \mathbf{k}_1=\mathbf{k}_2=\mathbf{k} \quad (3) \\ 1+g^{(2)}_{\mathrm{NG}}(\mathbf{k}_1, \mathbf{k}_2; t) & \mathbf{k}_1\neq\mathbf{k}_2 \quad (4) \end{cases}$$

where $\mathbf{k}_1$ and $\mathbf{k}_2$ are the two scattering vectors, corresponding to the positions of the detectors and β is a number of order unity. $g^{(2)}_{\mathrm{NG}}(\mathbf{k}_1, \mathbf{k}_2; t)$ can be factorized into a number fluctuation term, $g^{(2)\mathrm{T}}_{\mathrm{NG}}$, and an intramolecular term, $g^{(2)\mathrm{I}}_{\mathrm{NG}}$. Even when $\mathbf{k}_1$ and $\mathbf{k}_2$ are very similar, the second term on the right hand side of equation (3) is negligible[4], provided $|\mathbf{k}_1-\mathbf{k}_2|V^{1/3}\gg 1$, where V is the scattering volume.

Where the scattering particles are linear polymers we may consider the polymer chain to comprise N scattering centres ('beads')[20]. The intramolecular term then reflects four-bead correlations depending on the internal dynamics of the beads in one polymer chain. We consider here a bead-spring model of a polymer in which there are N beads and $N-1$ linkages between the beads. The coordinates of the 'beads' are given by:

$$\mathbf{r}_i=\sum_{\alpha=1}^{N-1} Q_{i\alpha}\boldsymbol{\mu}_\alpha \tag{5}$$

where the $\{\boldsymbol{\mu}_\alpha\}$ are the normal modes of the chain with relaxation times, τ_α, and the $\langle\mu_\alpha^2\rangle$ are the mean-square equilibrium mode lengths. The beads are supposed to be connected by Hookean springs of force constant $3k_BT/b^2$, where k_B is the Boltzmann constant, T is the absolute temperature and b is the rms length of a spring. Each bead has a frictional constant ρ for translational motion with respect to the solvent. The equations of motion are then as given by Zimm[21] (see also reference 5, equation (11)).

As shown by Pecora[22],

$$g^{(1)}(\mathbf{k}, t)=\frac{1}{N^2}\exp(-Dk^2t)$$

$$\times\sum_{ij}\exp\left[-\left(\sum_\alpha\frac{\langle\mu_\alpha^2\rangle k^2}{6}\{Q_{i\alpha}^2+Q_{j\alpha}^2-2Q_{i\alpha}Q_{j\alpha}\,\mathrm{e}^{-t/\tau_\alpha}\}\right)\right] \tag{6}$$

where D is the translational diffusion coefficient of the polymer chain.

The initial slope of $g^{(1)}$, $\mathrm{d}[g^{(1)}(\mathbf{k}, t)]/\mathrm{d}t|_{t=0}$ is given as:

$$\left.\frac{\mathrm{d}g^{(1)}(\mathbf{k}, t)}{\mathrm{d}t}\right|_{t=0}=-\frac{k^2}{N^2}$$

$$\times\sum_{ij}\exp\left(-\sum_\alpha\left[\frac{\langle\mu_\alpha^2\rangle k^2}{6}\{Q_{i\alpha}^2+Q_{j\alpha}^2-2Q_{i\alpha}Q_{j\alpha}\}\right]\right)$$

$$\times\left(D+\frac{1}{3}\sum_\alpha\frac{\langle\mu_\alpha^2\rangle}{\tau_\alpha}Q_{i\alpha}Q_{j\alpha}\right) \tag{7}$$

Similarly[5], $g^{(2)I}_{\mathrm{NG}}$ is expressed in terms of the coefficients $\{Q_{i\alpha}\}$ of the chain as:

$$g^{(2)I}_{\mathrm{NG}}(\mathbf{k}_1, \mathbf{k}_2; t)$$

$$=\frac{\left[\sum_{ijkl}\prod_\alpha\exp\left[-\frac{\langle\mu_\alpha^2\rangle}{6}(k_1^2Q_{ij\alpha}^2+k_2^2Q_{kl\alpha}^2+2\mathbf{k}_1.\mathbf{k}_2Q_{ij\alpha}Q_{kl\alpha}\,\mathrm{e}^{-t/\tau_\alpha})\right]\right]}{\left[\sum_{ij}\prod_\alpha\exp\left(-\frac{\langle\mu_\alpha^2\rangle}{6}k_1^2Q_{ij\alpha}^2\right)\right]\left[\sum_{ij}\prod_\alpha\exp\left(-\frac{\langle\mu_\alpha^2\rangle}{6}k_2^2Q_{ij\alpha}^2\right)\right]} \tag{8}$$

where the condensed notation

$$Q_{ij\alpha}=Q_{i\alpha}-Q_{j\alpha} \tag{9}$$

has been used. The slope, $\mathrm{d}(\log g^{(2)I}_{\mathrm{NG}})/\mathrm{d}t|_{t=0}$, is given by

$$\left.\frac{\mathrm{d}\log(g^{(2)I}_{\mathrm{NG}}(\mathbf{k}_1, \mathbf{k}_2; t))}{\mathrm{d}t}\right|_{t=0}=\mathcal{N}^{-1}\sum_{ijkl}\sum_\alpha\frac{\langle\mu_\alpha^2\rangle}{3\tau_\alpha}\mathbf{k}_1.\mathbf{k}_2Q_{ij\alpha}Q_{kl\alpha}$$

$$\times\exp\left[-\sum_\alpha\frac{\langle\mu_\alpha^2\rangle}{6}(\mathbf{k}_1^2Q_{ij\alpha}^2+\mathbf{k}_2^2Q_{kl\alpha}^2+2\mathbf{k}_1.\mathbf{k}_2Q_{ij\alpha}Q_{kl\alpha})\right] \tag{10}$$

where

$$\mathcal{N}=g^{(2)I}_{\mathrm{NG}}(\mathbf{k}_1, \mathbf{k}_2; 0)\left[\sum_{ij}\prod_\alpha\exp\left(-\frac{\langle\mu_\alpha^2\rangle}{6}\mathbf{k}_1^2Q_{ij\alpha}^2\right)\right]$$

$$\times\left[\sum_{ij}\prod_\alpha\exp\left(-\frac{\langle\mu_\alpha^2\rangle}{6}\mathbf{k}_2^2Q_{ij\alpha}^2\right)\right] \tag{11}$$

The Rouse model for a flexible polymer

In the Rouse model the eigenvalues, λ_α, are given by[6]

$$\lambda_\alpha=4\sin^2\left[\frac{\alpha\pi}{2N}\right] \qquad \alpha=1, 2, \ldots, N-1 \tag{12}$$

and we have

$$\langle\mu_\alpha^2\rangle=b^2/\lambda_\alpha \tag{13}$$

For a Rouse chain[22]

$$\tau_\alpha=b^2/3NDk\lambda_\alpha \tag{14}$$

where b is given by[9]

$$b=R_g[6/(N-1)]^{1/2} \tag{15}$$

R_g being its radius of gyration. (In Zimm's notation, as in equation (38) of ref. 21, our relaxation times, τ_α, are given by $(\sigma\lambda_\alpha)^{-1}$.) The $Q_{i\alpha}$ are given by[23]:

$$Q_{i\alpha}=\left(\frac{2}{N}\right)^{1/2}\cos\left[\frac{\pi\alpha(i-1/2)}{N}\right] \qquad i=1, 2, \ldots, N \tag{16}$$

For the sake of definiteness we have taken as D for the Rouse model the value obtained by assuming the polymer behaves as a Stokes–Einstein sphere of radius equal to R_g, i.e.

$$D=\frac{k_BT}{6\pi\eta R_g} \tag{17}$$

where η is the viscosity of the solvent. $g^{(1)}(\mathbf{k}, 0)$ and $g^{(2)}(\mathbf{k}, \mathbf{k}, 0)$ and their initial slopes were evaluated explicitly by fourfold summation over the N beads using equations (6)–(17). The results are described in the next section. (Note that in the case of the Rouse model, the initial slopes of $g^{(1)}$ and $g^{(2)}$ are proportional to D.)

Because of the orthonormality of the chosen $Q_{i\alpha}$ for the Rouse model, the expression in equation (10) may be simplified to give[5]

$$\frac{\mathrm{d}\log(g_{\mathrm{NG}}^{(2)I}(\mathbf{k}_1, \mathbf{k}_2; t)}{\mathrm{d}t} = \mathcal{N}^{-1} D\mathbf{k}_1.\mathbf{k}_2 \sum_{ijkl} \times \exp\left[-\sum_{\alpha}\left(\frac{\langle\mu_\alpha^2\rangle}{6}[k_1^2 Q_{ij\alpha}^2 + k_2^2 Q_{kl\alpha}^2 + 2\mathbf{k}_1.\mathbf{k}_2 Q_{ij\alpha}Q_{kl\alpha}]\right)\right] \times (\delta_{ik} - \delta_{il} - \delta_{jk} + \delta_{jl}) \quad (18)$$

where the δ_{ij} are Kronecker deltas.

Another approach to evaluating equation (6), for $kb \ll 1$, is to approximate the sums from 1 to N by integrating analytically from 0 to N. Substituting in equation (6), for large N, approximate forms of the eigenvalues,

$$\lambda_\alpha = \frac{\alpha^2\pi^2}{N^2} \quad (19)$$

and of the $Q_{i\alpha}$,

$$Q_{i\alpha} = \left(\frac{2}{N}\right)^{1/2} \cos\left[\pi\alpha\left(\frac{i}{N} - \frac{1}{2}\right)\right] \quad \alpha \text{ even} \quad (20)$$

$$= \left(\frac{2}{N}\right)^{1/2} \sin\left[\pi\alpha\left(\frac{i}{N} - \frac{1}{2}\right)\right] \quad \alpha \text{ odd}$$

$$(\alpha = 1, 2, \ldots, N-1)$$

we obtain the Debye expression for $g^{(1)}(\mathbf{k}, 0)$ (ref. 20):

$$g^{(1)}(\mathbf{k}, 0) = \frac{2}{k^4 R_g^4}[k^2 R_g^2 - 1 + \exp(-k^2 R_g^2)] \quad (21)$$

Equations (8) and (18) were evaluated analytically by approximating sums by integrals in a similar way (see equations 15 and 16 in ref. 5) to give $g^{(2)}(\mathbf{k}, \mathbf{k}; 0)$:

$$g^{(2)}(\mathbf{k}, \mathbf{k}; 0) = \mathcal{N}^{-1}\left(\frac{87}{2k^8R_g^8} - \frac{30}{k^6R_g^6} + \frac{8}{k^4R_g^4} - \frac{392}{9k^8R_g^8} \times \exp(-k^2R_g^2) - \frac{40}{3k^6R_g^6}\exp(-k^2R_g^2) + \frac{1}{18k^8R_g^8}\exp(-4k^2R_g^2)\right) \quad (22)$$

where $\mathcal{N} = [g^{(1)}(\mathbf{k}, 0)]^2$, $g^{(1)}(\mathbf{k}, 0)$ being given by equation (21) and the initial slope of $g^{(2)}(\mathbf{k}, \mathbf{k}, 0)$ by:

$$\left.\frac{\mathrm{d}(g_{\mathrm{NG}}^{(2)I}(\mathbf{k}, \mathbf{k}; t))}{\mathrm{d}t}\right|_{t=0} = \mathcal{N}^{-1} Dk^2\left[\frac{10}{k^4R_g^4} - \frac{4}{k^2R_g^2} + \frac{32}{3k^6R_g^6} \times [\exp(-k^2R_g^2) - 1] - \frac{1}{6k^6R_g^6}(\exp\{-4k^2R_g^2\} - 1)\right] \quad (23)$$

Equations (22) and (23) agree with the results of Pusey[4].

Hearst approximation of the Zimm model

Here it is assumed that the free-draining eigenfunctions, $Q_{i\alpha}$, given by Zimm[21] for a continuous chain may be used as approximations for the eigenfunctions in the discrete case for $0 < h < \infty$, where h is the draining parameter; h is related to the frictional coefficient of each bead, ρ, as defined by Zimm[21]:

$$h = N^{1/2}\rho/(12\pi^3)^{1/2}b\eta \quad (24)$$

where ρ is the friction constant of each statistical segment and b is given by equation (15). The $Q_{i\alpha}$ are as given in equation (20). The mean-square equilibrium mode lengths are given by equation (13). In the free-draining case ($h \to 0$) the eigenvalues, λ_α, are given by equation (19). For non-zero values of h, the eigenvalues, λ_α, within the Hearst approximation[24] are the sum of free-draining and non-draining contributions:

$$\lambda_\alpha = \frac{\pi^2}{N^2}\left(\alpha^2 + 4h\frac{\lambda'_\alpha}{\pi^2}\right) \quad (25)$$

As described by Hearst[24], for $\alpha \leqslant 8$, λ'_α was set equal to the diagonal elements of the matrix G given in Table 1 of Zimm *et al.*[25], while for $\alpha \geqslant 9$, $2\lambda'_\alpha/\pi^2$ was set equal to $\alpha^{3/2}$. The relaxation times are given by:

$$\tau_\alpha = \frac{b^2\rho}{3k_BT\lambda_\alpha} \quad (26)$$

(The relaxation times, τ_α, are given by $(\sigma\lambda_\alpha)^{-1}$, using Zimm's notation[21], as for the Rouse model.) In the Zimm limit of $h \to \infty$, the relaxation times, τ_α, are given by[21,24,25]

$$\tau_\alpha = \frac{\eta b^3[(N-1)\pi]^{3/2}}{12^{1/2}k_BT\lambda'_\alpha} \quad (27)$$

According to Bloomfield and Zimm[26] the translational diffusion coefficient for a straight chain flexible macromolecule is given by:

$$D = \frac{k_BT}{N\rho}\left[1 + \frac{\rho}{6\pi\eta(N-1)}\left(\sum_{i=1}^{N}\sum_{j=1}^{i-1}\left(\frac{6}{\pi b^2(i-j)}\right)^{1/2} + \sum_{i=1}^{N}\sum_{j=i+1}^{N}\left(\frac{6}{\pi b^2(j-i)}\right)^{1/2}\right)\right] \quad (28)$$

In the limit of $\rho \to \infty$ ($h \to \infty$) the first term can be neglected. *Figure 1a* shows the N-dependence of D, which approaches at large N the value obtained by converting the double sums to integrals, $4k_BT/(9\pi^{3/2}\eta R_g)$ (equation 67 of Bloomfield and Zimm[26]). It may be seen that, even for $N = 100$, the maximum value for N used in our calculations of the correlation functions for the Zimm model, D lies below this asymptotic value. For consistency, therefore, in our calculations of $g^{(1)}$ and $g^{(2)}$ we computed $D(N)$ using equation (28). The h-dependence of D calculated from equation (28) closely follows the h-dependence given by the analytical expression for $D(h)$ derived by Kirkwood within the pre-averaging approximation. *Figure 1b* shows the dependence of D on h, obtained from the integral formula:

$$D = \frac{k_BT}{6R_gh\eta(2\pi^3)^{1/2}} + \frac{4k_BT}{9\pi^{3/2}R_g\eta} \quad (29)$$

which is the result obtained using the Kirkwood approximation (ref. 27, see also p. 279 of ref. 9). As $h \to \infty$ the first term is clearly negligible as with equation (28); as $h \to 0$ the first term becomes infinitely large. Despite this unphysical behaviour of $D(h)$, at $h = 0$ the values of the chain correlation functions for small h interpolate sensibly between Rouse and Zimm limits (see next section).

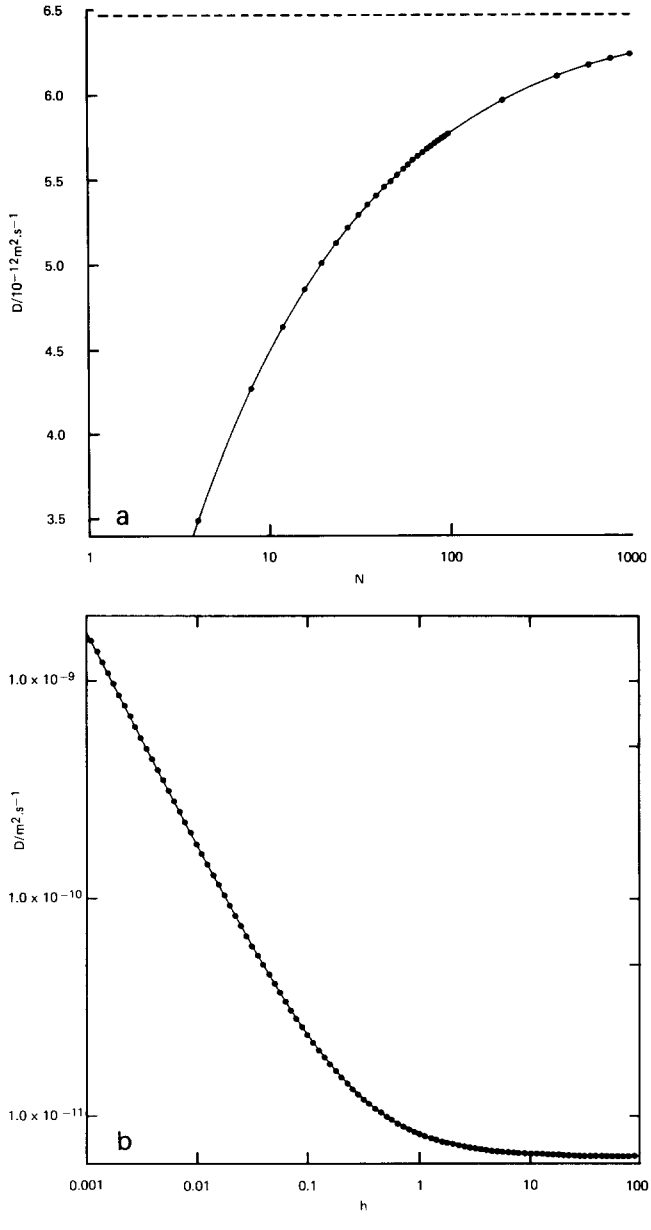

Figure 1 (a) Diffusion coefficient (——) of a Zimm polymer ($h \to \infty$) of radius of gyration, R_g, of 50 nm in a solvent of viscosity, η, of 1.0 mPa s as a function of the number of beads, N. (– – – –), $4k_BT/(9\pi^{3/2}\eta R_g)$. (b) Diffusion coefficient of a Zimm polymer of radius of gyration, R_g, of 50 nm in a solvent of viscosity, η, of 1.0 mPa s for $N \to \infty$ as a function of the draining parameter, h

RESULTS

Calculations of $g^{(1)}(\mathbf{k}, t)$ and $g^{(2)}(\mathbf{k}, \mathbf{k}; t)$ were carried out for a range of values of N and k, R_g being fixed at 50 nm. The distance scales that are observable in a light scattering experiment are of the order of k^{-1}; results are therefore presented as functions of kR_g, and kb.

The Rouse model[6]

For the Rouse model, the mean-square equilibrium mode lengths, the normal modes, their relaxation times and eigenvalues, the distance between the beads and the diffusion coefficient are given by equations (12)–(17).

Calculations of $g^{(1)}$. For various values of N, up to $N = 300$, $g^{(1)}(\mathbf{k}, 0)$ was computed explicitly as a function of $\mathbf{k}$ by carrying out the two-fold summation in equation (6), making the appropriate substitutions. Selected values are given in *Table 1*. At low values of kR_g (for $kb \ll 2$), $g^{(1)}(\mathbf{k}, 0)$ was found to be well approximated by the Debye expression (21). As kR_g increased, the value for $g^{(1)}(\mathbf{k}, 0)$ diverged from the Debye value, being smaller by approximately 5% for $kb = 1$. As $kR_g \to \infty$, $g^{(1)}(\mathbf{k}, 0) \to N^{-1}$, whereas the Debye value for $g^{(1)}(\mathbf{k}, 0)$ tends to zero.

In *Figure 2* we show the first cumulant of $g^{(1)}(\mathbf{k}, t)$, Φ ($\Phi = -\mathrm{d}\log(g^{(1)}(\mathbf{k}, t))/\mathrm{d}t|_{t=0}$), computed from equations (6) and (7), as a function of kR_g for a range of values of N. We obtained limiting values of $\Phi \to Dk^2$ as $kR_g \to 0$, and $\Phi \to NDk^2$ as $kR_g \to \infty$; Akcasu *et al.*[28] reported similar results for $N = 101$ for a Gaussian ring polymer. Schaefer and Han[29] indicated that, from scaling arguments, the expected relaxation rates were $\Phi = Dk^2$ for $kR_g \ll 1$, and $\Phi = D_m k^2$ for $kR_g \approx 1$, where D_m is the monomer translational diffusion coefficient, which is equal to ND, in agreement with our findings.

Calculations of $g^{(2)}$. At low values of kR_g, $g^{(2)}(\mathbf{k}, \mathbf{k}; 0)$ obtained from equation (8), making substitutions from equations (12)–(17) (explicit sums), was in good agreement with that obtained from equation (22) (approximation by integrals). Selected values are given in *Table 2* (NB the five sum expression (8) was in general not evaluated for $N > 30$ because of the excessive computing times required.) At $kb = 2$, the value of $g^{(2)}(\mathbf{k}, \mathbf{k}; 0)$

Table 1 Values of $g^{(1)}(\mathbf{k}, 0)$ for the Rouse model

kR_g	$N =$ 8	20	100	300	$g^{(1)}(\mathbf{k}, 0)^a$ (Debye)
0.1	0.9963	0.9965	0.9967	0.9967	0.9967
1	0.7118	0.7257	0.7358	0.7358	0.7358
2	0.3573	0.3660	0.3774	0.3773	0.3773
4	0.1492	0.1190	0.1175	0.1172	0.1172
10	0.1250	0.0505	0.0215	0.0200	0.0198
60	0.1250	0.0500	0.0100	0.0033	0.0006
100	0.1250	0.0500	0.0100	0.0033	0.0002

[a] Values of $g^{(1)}(\mathbf{k}, 0)$ obtained from equation (21)

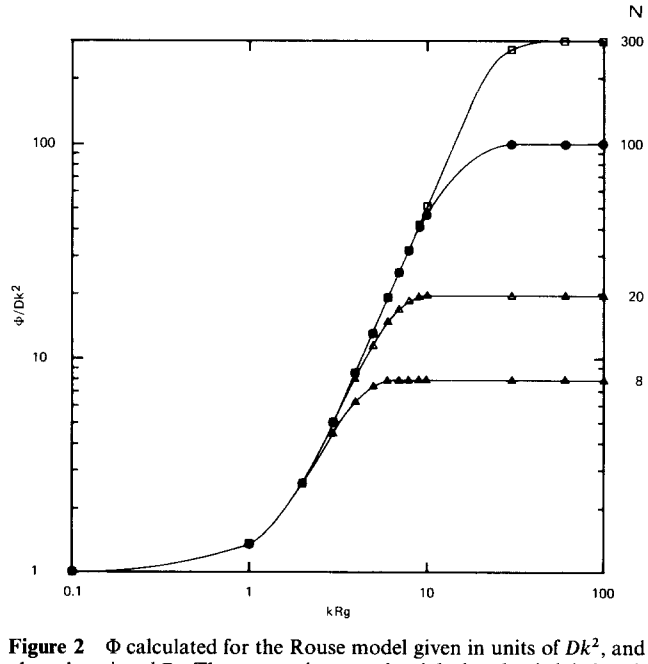

Figure 2 Φ calculated for the Rouse model given in units of Dk^2, and plotted against kR_g. The annotations on the right hand axis label each curve with the corresponding value of N used in the calculations

Table 2 Values of $g^{(2)}(\mathbf{k}, \mathbf{k}; 0)$ for the Rouse model

kR_g	$N=$ 8	20	30	$g^{(2)}(\mathbf{k}, \mathbf{k}; 0)^a$ (Debye)
0.1	1.000	1.000	1.000	1.000
1	1.075	1.064	1.058	1.058
2	1.432	1.386	1.366	1.365
4	1.825	1.811	1.796	1.791
10	1.875	1.949	1.962	1.965
60	1.875	1.950	1.967	1.999
100	1.875	1.950	1.967	2.000

[a] Values of $g^{(2)}(\mathbf{k}, \mathbf{k}; 0)$ obtained from equation (22)

obtained from equation (8) was slightly larger than that obtained from equation (22) (by 10% for $N=4$; the difference decreases with increasing N). For $kb \geqslant 8.5$, $g^{(2)}(\mathbf{k}, \mathbf{k}; 0) = 2 - N^{-1}$. By contrast equation (22) gives a value of 2 in the limit $kR_g \to \infty$, the same result as we obtained earlier by a method of numerical integration[5]. Thus, at large kR_g, the values of $g^{(2)}(\mathbf{k}, \mathbf{k}; 0)$ obtained from equation (8) were lower than the corresponding values from equation (22).

In *Figure 3a* we have plotted the normalized initial slope of $g^{(2)}$, as

$$\Gamma = \frac{-\lim_{t \to 0} \frac{\mathrm{d}}{\mathrm{d}t} [g_{NG}^{(2)I}(\mathbf{k}_1, \mathbf{k}_2; t)]}{g_{NG}^{(2)I}(\mathbf{k}_1, \mathbf{k}_2; 0) - 1} \qquad (30)$$

(in units of D/R_g^2) against kR_g for a range of values of N. Γ was calculated from equation (30), substituting in the value for $\mathrm{d}(g^{(2)}(\mathbf{k}, \mathbf{k}; t))/\mathrm{d}t|_{t=0}$ obtained from equation (18). (Equation (18) contains four four-sum expressions, while equation (10) is a five-sum expression. Equation (18) is therefore faster to compute.) For $N \leqslant 30$ $g^{(2)}(\mathbf{k}, \mathbf{k}; 0)$ was calculated from equation (8). For $N > 30$ $g^{(2)}(\mathbf{k}, \mathbf{k}; 0)$ was estimated as follows. For $kb \leqslant 2$, $g^{(2)}(\mathbf{k}, \mathbf{k}; 0)$ was calculated using equation (22). In the next section we show that $g^{(2)}(\mathbf{k}, \mathbf{k}; 0)$ obtained for the Hearst approximation of the Zimm model approaches $g^{(2)}(\mathbf{k}, \mathbf{k}; 0)$ for the Rouse model as N increases (*Tables 2* and *5*). For $kb > 2$, and $30 < N \leqslant 100$, therefore, $g^{(2)}(\mathbf{k}, \mathbf{k}; 0)$ was approximated by the value obtained for the Zimm model (calculations described in full in the next section). For $kR_g \geqslant 30$ (corresponding to $kb \geqslant 4.3$) and $N = 300$ $g^{(2)}(\mathbf{k}, \mathbf{k}; 0)$ was taken to be $2 - 1/300$. We have also plotted, for comparison, Γ_{int}, defined as Γ calculated from equations (21)–(23) and (30).

Figure 3a shows that Γ was nearly constant, for a given value of N, for $kR_g \ll 1$. In *Table 3* we give values for Γ for a range of values of N and kR_g. The value of Γ tends to 15 as $N \to \infty$ and $kR_g \to 0$, in agreement with Pusey[4] (the break in the trend for Γ observable in *Table 3* at $kR_g = 0.1$ results from the change from calculation of $g^{(2)}(\mathbf{k}, \mathbf{k}; 0)$ using equation (8) to estimation of $g^{(2)}(\mathbf{k}, \mathbf{k}; 0)$ for $N > 30$, as described above). *Figure 3b* shows the same data with Γ given in units of Dk^2. The computed curves show a crossover region at $kR_g \approx 1$, where Γ starts to increase with kR_g. For the values derived from the sums, the power dependence of Γ on kR_g goes through a maximum as kR_g is increased, while the integral formulae (equations (21)–(23)) give $\Gamma \propto (kR_g)^4$ for $kR_g \gg 1$. The gradients of the curves for the numerical sums show a dependence of Γ on $(kR_g)^2$ at high values of kR_g (for $kb > 6$). The value of Γ was found to be equal to $2NDk^2$.

At constant kR_g, as N increased, the value for Γ obtained by explicit summation became closer to the value obtained from the integral formulae. The deviation between the two values was more marked for $kb > 2$ (in a real experiment information would only be revealed

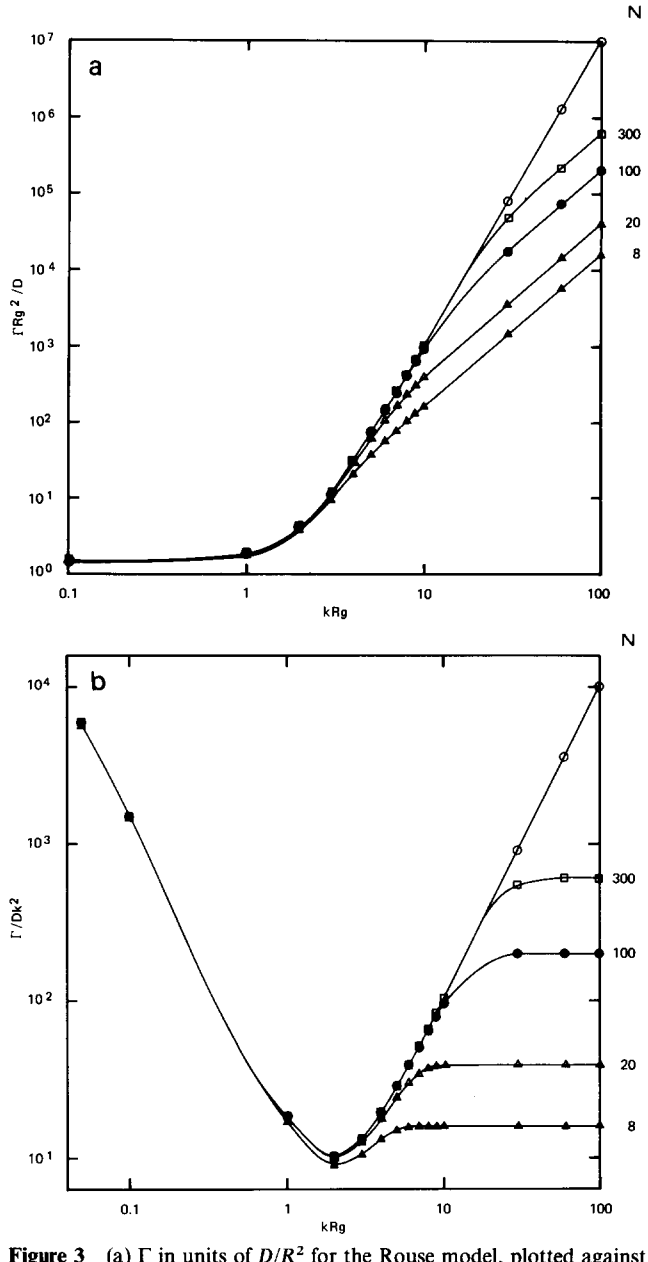

Figure 3 (a) Γ in units of D/R_g^2 for the Rouse model, plotted against kR_g. The annotations on the right hand axis label each curve with the corresponding value of N used in the calculations, while the top, unannotated, curve shows Γ_{int} calculated from equations (21)–(23) and (30). (b) Γ in units of Dk^2 for the Rouse model, plotted against kR_g. The same symbols are used as in (a).

Table 3 Values of Γ for the Rouse model, in units of D/R_g^2

kR_g	$N=$ 8	20	100	300	Γ_{int}[a]
0.1	12.46	14.15	15.17	15.07	15.02
1	15.57	17.54	18.42	18.43	18.43
2	36.49	40.50	41.30	41.32	41.32
4	221.3	297.5	313.6	314.5	314.6
10	1600	3963	9478	1.02×10^4	1.03×10^4
60	5.76×10^4	1.44×10^5	7.20×10^5	2.17×10^6	1.30×10^7
100	1.60×10^5	4.00×10^5	2.00×10^6	6.04×10^6	1.00×10^8

[a] Values obtained from equations (21)–(23), and (30)

about internal modes on a length scale greater than the minimum which could be probed by the radiation: k^{-1}). The point at which the numerical and analytical results came into close agreement corresponds with the point at which $kb=2$. Clearly it is not necessary to satisfy the condition $kb \ll 1$ in order for the approximation

$$\sum_{1}^{N} \approx \int_{0}^{N} \tag{31}$$

to hold true. The transition at $kb=2$ has a physical meaning because it corresponds to the point where the distance between the beads is twice the length scale being probed. This result is reminiscent of the Nyquist sampling theorem[30], which states, roughly speaking, that equi-spaced data, with two or more points per cycle of the highest frequency, allow reconstruction of a function, whose Fourier transform is very small outside some finite interval (a band limited function). In the present case the 'data' correspond to points on a grid whose spacing is defined by the k^{-1} length scale and the band limited function describes the chain conformation.

In the limit $kR_g \to \infty$, the inverse scattering vector is much smaller than the size of the polymer coil and the scattered light field becomes a complex Gaussian variable[4]. Under this condition $g^{(2)}(\mathbf{k}, \mathbf{k}; t)$ can be factorized and expressed in terms of $g^{(1)}(\mathbf{k}, t)$, and Γ can be expressed in terms of $\mathrm{d}(g^{(1)}(\mathbf{k}, t))/\mathrm{d}t|_{t=0}$ and $g^{(2)}(\mathbf{k}, \mathbf{k}; 0)$[4]:

$$\lim_{kR_g \to \infty} \Gamma = -2 \left. \frac{\mathrm{d}(g^{(1)}(\mathbf{k}, t))}{\mathrm{d}t} \right|_{t=0} / (g^{(2)I}_{NG}(\mathbf{k}, \mathbf{k}; 0) - 1) \tag{32}$$

In addition to our explicit calculations of Γ, therefore, we also calculated an estimated value for Γ from equation (32), Γ_{est}, and compared Γ_{est} with Γ. For all N and for $kb \geqslant 6$, we found that $\Gamma = -2\mathrm{d}(g^{(1)}(\mathbf{k}, t))/\mathrm{d}t|_{t=0}$, and the ratio Γ_{est}/Γ was $1+(N-1)^{-1}$. For $kR_g > 4$, Γ_{est}/Γ was within 10% of the value of $1+(N-1)^{-1}$, reaching this value exactly as kR_g increased. Thus the Gaussian factorization is found to be an approximation appropriate for large N and $kR_g > 4$. We therefore predict that as $kR_g \to \infty$, the dependence of Γ on kR_g will be the same as for Φ. In *Figure 5b* Γ and Γ_{est} are shown against kR_g for $N=100$. However, it is clear from this figure that Γ shows (approximately) the power dependence on kR_g predicted theoretically ($(kR_g)^4$ for the Rouse case) only over a narrow region of kR_g space. Γ_{est} and Γ are not exactly coincident in this region.

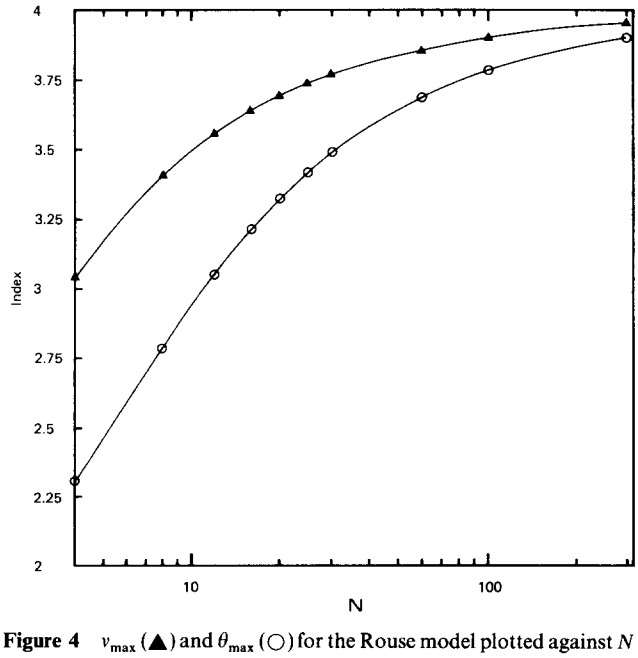

Figure 4 ν_{max} (▲) and θ_{max} (○) for the Rouse model plotted against N

Table 4 Values of $g^{(1)}(\mathbf{k}, 0)$ for the Zimm model, Hearst approximation

kR_g	$N=$ 8	20	60	100
0.1	0.9966	0.9966	0.9967	0.9967
1	0.7346	0.7338	0.7349	0.7352
2	0.3963	0.3815	0.3782	0.3778
4	0.1731	0.1344	0.1221	0.1200
10	0.1250	0.0519	0.0278	0.0241
60	0.1250	0.0500	0.0167	0.0100
100	0.1250	0.0500	0.0167	0.0100

Table 5 Values of $g^{(2)}(\mathbf{k}, \mathbf{k}; 0)$ for the Zimm model, Hearst approximation

kR_g	$N=$ 8	20	60	100
0.1	1.000	1.000	1.000	1.000
1	1.071	1.063	1.059	1.059
2	1.411	1.383	1.371	1.368
4	1.798	1.800	1.794	1.793
10	1.875	1.947	1.964	1.965
60	1.875	1.950	1.983	1.990
100	1.875	1.950	1.983	1.990

In order to obtain the maximum power dependence of Γ on kR_g, θ_{max}, the slope of the double logarithmic plot of Γ against kR_g, θ, was determined numerically for each pair of adjacent values of kR_g. θ_{max} was determined to an accuracy of better than 0.5% by a process of progressive subdivision, and is plotted against N in *Figure 4*. For comparison we have also shown in this graph the maximum power dependence of Φ on kR_g, ν_{max}; ν_{max} was greater than θ_{max} for all values of N investigated. It may be seen that, even for $N=100$, the dependence of Γ on kR_g was found to be appreciably less than the fourth power dependence of Φ on kR_g predicted theoretically by de Gennes[31] for the Rouse chain although both ν_{max} and θ_{max} approach 4 as $N \to \infty$.

The Zimm model[21] *(Hearst approximation*[24]*)*

For the Hearst approximation of the Zimm model, the mean-square equilibrium mode lengths are given, as for the Rouse model, by equation (13), the modes are given by equation (20), the eigenvalues by equation (19), the distance between the beads by equation (15) and the diffusion coefficient by equation (28).

The limit $h \to \infty$

In the limit $h \to \infty$, the relaxation times are given by equation (27).

The results of the numerical calculations of the static values, $g^{(1)}(\mathbf{k}, 0)$ and $g^{(2)}(\mathbf{k}, \mathbf{k}; 0)$, for the Zimm model, given in *Tables 4* and *5*, were compared with those obtained for the Rouse model (*Tables 1* and *2*). The differences between the Rouse and the Zimm models lie mainly in their dynamic rather than static properties, and, if the Hearst approximation for the Zimm model is good, these static values should be identical at large N. At small values of kR_g ($kb \ll 1$), and at large values of kR_g ($kb \geqslant 8$) there was good agreement between the two

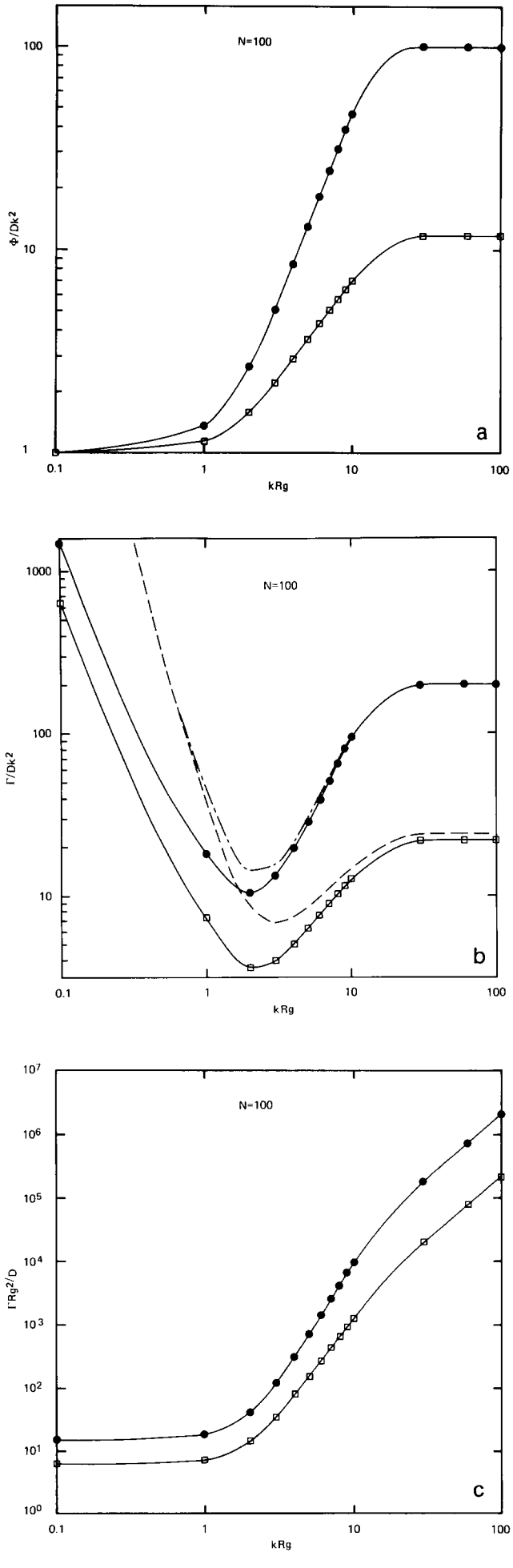

sets of values. For intermediate values of kb, we computed the ratios of the values of $g^{(1)}(\mathbf{k}, 0)$ and $g^{(2)}(\mathbf{k}, \mathbf{k}; 0)$ calculated from the Hearst approximation to those calculated from the Rouse model. For $g^{(1)}(\mathbf{k}, 0)$, the ratio went through a maximum (of 1.2 for $N=4$) at $kb \approx 2.8$; by contrast, for $g^{(2)}(\mathbf{k}, \mathbf{k}; 0)$, the ratio went through a minimum (of 0.95 for $N=4$) in the same region. As N is increased the two sets of values approached one another; the ratio for $g^{(1)}(\mathbf{k}; 0)$ approached 1.000 much more slowly than that for $g^{(2)}(\mathbf{k}, \mathbf{k}; 0)$. Since $g^{(1)}(\mathbf{k}, 0)$ is used in the calculation of $g^{(2)}(\mathbf{k}, \mathbf{k}; 0)$ (equation (2)), and, in all cases the Rouse and Hearst values of $g^{(2)}(\mathbf{k}, \mathbf{k}; 0)$ are in closer agreement than the Rouse and Hearst values of $g^{(1)}(\mathbf{k}; 0)$, errors arising from the Hearst approximation must, to some extent, cancel out in the calculation of $g^{(2)}$.

To calculate Γ from equation (30), it was necessary to obtain $d(g^{(2)}(\mathbf{k}, \mathbf{k}; t))/dt|_{t=0}$ from equation (10). In *Figures 5a, b* and *c* we compare Φ and Γ calculated for $N=100$ for the Rouse and Zimm models. ν_{max} and θ_{max} are plotted against N in *Figure 6*. The values of both are clearly lower for the Zimm model than for the Rouse model for all values of N. As with the Rouse model, $\Phi \rightarrow Dk^2$ as $kR_g \rightarrow 0$ and $g^{(2)}(\mathbf{k}, \mathbf{k}; 0)$ tends to unity. Φ and Γ for the Zimm model vary as $(kR_g)^2$ at large values of kR_g, and for $kR_g > 0$, $\Phi_{Zimm} < \Phi_{Rouse}$ and $\Gamma_{Zimm} < \Gamma_{Rouse}$. We found, for $kR_g/N \leqslant 1 \times 10^{-3}$, that the denominator of equation (30), $(g^{(2)}(\mathbf{k}, \mathbf{k}; 0) - 1)$, was subject to significant rounding errors, causing an overestimate in the value of Γ. For $N=100$, and $kR_g = 0.1$, Γ was approximated, therefore, by substituting in the denominator of equation (30) the value of $g^{(2)}(\mathbf{k}, \mathbf{k}; 0)$ obtained for the Rouse model from equation (22). For $kR_g \rightarrow 0$ and for pre-averaged Oseen hydrodynamics Pusey[4] gave a value of $\Gamma = 39/7$ (in units of D/R_g^2). For the values of N used, we found that, for

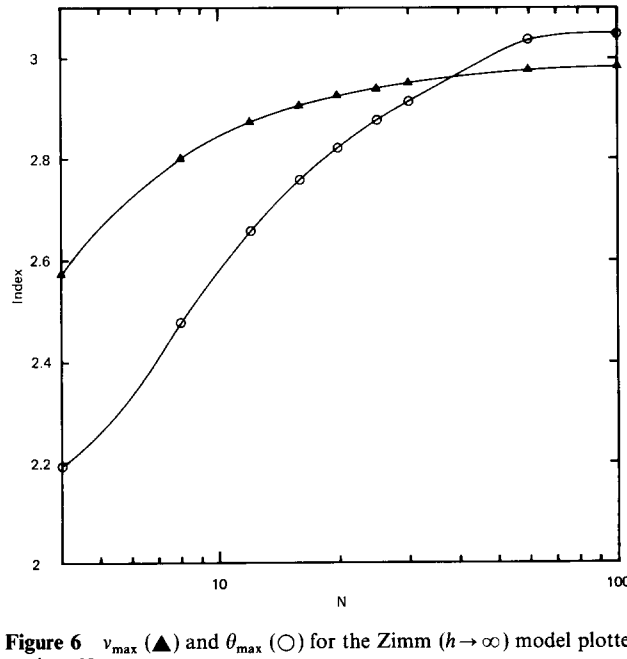

Figure 6 ν_{max} (▲) and θ_{max} (○) for the Zimm ($h \rightarrow \infty$) model plotted against N.

Figure 5 (a) Φ for the Rouse (●) and the Zimm ($h \rightarrow \infty$) (□) models in units of Dk^2 plotted against kR_g for $N=100$. (b) Γ for the Rouse (●) and the Zimm ($h \rightarrow \infty$) (□) models, and Γ_{est} for the Rouse (– – – –) and for the Zimm (——) models in units of Dk^2 plotted against kR_g for $N=100$. (c) Γ for the Rouse (●) and the Zimm ($h \rightarrow \infty$) (□) models in units of D/R_g^2 plotted against kR_g for $N=100$

$kR_g < 5$, Γ decreased with increasing N; for $kR_g = 0.1$ and $N < 100$, $\Gamma = 39/7 + 14.3N^{-0.682}$.

In the long chain, non-draining limit, for $kR_g \to \infty$ and for pre-averaged Oseen hydrodynamics the initial slope of $g^{(1)}(\mathbf{k}, t)$, $d(g^{(1)}(\mathbf{k}, t))/dt|_{t=0}$ was predicted theoretically to be $-k^3 k_B T/6\pi\eta$ (ref. 28). From $D = 4k_B T/(9\pi^{3/2}\eta R_g)$ (see equation (29)) we obtain $d(g^{(1)}(\mathbf{k}, t))/dt|_{t=0} = -3\pi^{1/2}(kR_g)^3/8$ (in units of D/R_g^2) and hence, from equation (32), $\Gamma = 3\pi^{1/2}(kR_g)^3/4$. In our calculations for finite N, for $kR_g \geqslant 5$, Γ increased with increasing N. As kb decreased with increasing N to the value of 2, Γ appeared to approach $3\pi^{1/2}(kR_g)^3/4$. However, as kb increased the dependence of Φ and Γ on kR_g decreased to a quadratic dependence for $kb \geqslant 6$. For $N = 100$ and $kR_g \to \infty$, Φ was equal to $11.9(kR_g)^2$.

Γ_{est} was calculated from equation (32) for the Zimm model and is plotted against kR_g in *Figure 5b*. The ratio Γ_{est}/Γ was constant for $kb \geqslant 8$, and was larger than for the Rouse model for all values of N up to 100, having a value of approximately $(1 + N^{-1/2})$ (for $N = 100$, $\Gamma_{est}/\Gamma = 1.091$). For this model, also, the Gaussian factorization is appropriate for large values of N. The agreement between Γ_{est} and Γ is not as good as for the Rouse model. Γ shows (approximately) the theoretically predicted ($\approx (kR_g)^3$) dependence only over a narrow region of kR_g space.

As $N \to 100$, *Figure 6* shows that ν_{max} approached 3.00; this would be predicted from the Gaussian factorization, as discussed by Pusey[4]; however, θ_{max} approached 3.04. We do not know the reason for this anomaly, which presumably derives from imperfections of the Hearst approximation. Problems with the Hearst approximation may also be indicated by the decrease in Γ with increasing N, up to $N = 100$, for $kR_g < 5$ (see *Table 6*) which contrasts with the behaviour observed for the Rouse model (see *Table 3*).

Finite values of h

For finite values of h, the relaxation times are given by equation (26).

We have also carried out calculations of $g^{(1)}(\mathbf{k}, t)$ and $g^{(2)}(\mathbf{k}, \mathbf{k}; t)$ for a range of values of h. Selected numerical results are given in *Table 7* for $N = 100$. For $kR_g \to 0$, $\Phi = Dk^2$ for all values of h. At high values of kR_g ($kR_g = 100$), the Zimm ($h \to \infty$) limit gives $\Phi = 11.9(kR_g)^2$ (see previous section) and the Rouse model gives $\Phi = 100(kR_g)^2$ (*Table 3*). As h increases from 0.01 to 50, Φ decreases smoothly from $97.6(kR_g)^2$ to $12.4(kR_g)^2$ (*Table 7*). In the calculation of Γ at $kR_g = 0.1$ $g^{(2)}(\mathbf{k}, \mathbf{k}; 0)$ was approximated by the value obtained for the Rouse model from equation (22), as described in the previous section. $\Gamma(kR_g = 0.1)$ for $h \to \infty$ (*Table 6*) is 6.38; as h decreases, $\Gamma(kR_g = 0.1)$ increases monotonically (*Table 7*), approaching the value of 15.2 obtained for the Rouse model for $N = 100$ (*Table 3*) as $h \to 0$. From *Figure 7* and *Table 7* it can be seen that ν_{max} and θ_{max} obtained for $N = 100$ change smoothly in the transition from the Rouse model to the Zimm ($h \to \infty$) limit, the values of ν_{max} and θ_{max} decreasing monotonically with increasing h. The curves for ν_{max} and θ_{max} against h cross over at approximately $h = 1$.

Γ_{est} was calculated from equation (32) and the limiting ratio Γ_{est}/Γ at large kR_g is given against h in *Table 7*. A smooth increase of Γ_{est}/Γ from 1.010 (the same value as was obtained for the Rouse model) to 1.088 is observed as h is increased from 0.01 to 50; in the Zimm ($h \to \infty$) limit $\Gamma_{est}/\Gamma = 1.091$. Thus all the light scattering properties presented here for intermediate values of h show behaviour varying monotonically between the Rouse and Zimm limits.

Table 6 Values of Γ for the Zimm model, Hearst approximation, $h \to \infty$, in units of D/R_g^2

kR_g	$N =$ 8	20	60	100
0.1	9.06	7.42	6.44	6.38
1	10.5	8.64	7.55	7.27
2	21.15	17.23	14.91	14.31
4	102.1	93.87	83.30	80.10
10	762.6	1040	1254	1270
60	2.75×10^4	3.84×10^4	6.23×10^4	7.91×10^4
100	7.63×10^4	1.07×10^5	1.73×10^5	2.20×10^5

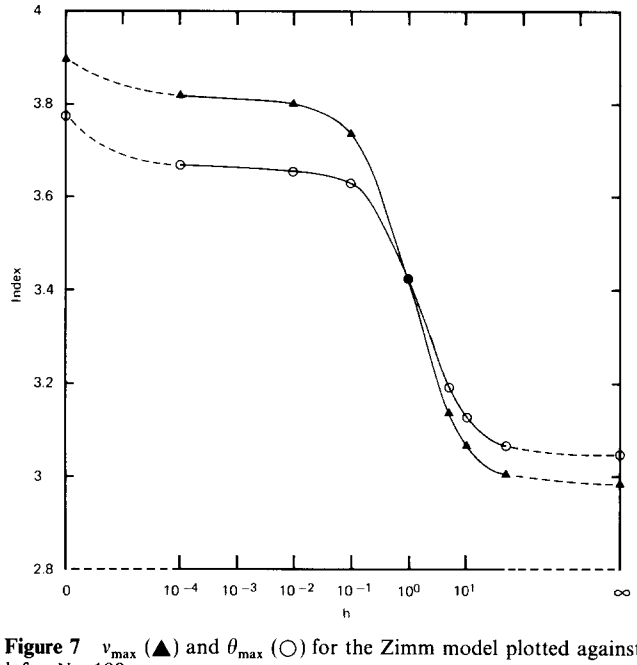

Figure 7 ν_{max} (▲) and θ_{max} (○) for the Zimm model plotted against h for $N = 100$

Table 7 Results from the Zimm model, Hearst approximation, finite h, for $N = 100$*

h	0.01	0.1	1	5	50
Φ ($kR_g = 0.05$)	2.5×10^{-3}	2.5×10^{-3}	2.5×10^{-3}	2.5×10^{-3}	2.5×10^{-3}
Φ ($kR_g = 100$)	9.76×10^5	7.82×10^5	3.22×10^5	1.69×10^5	1.24×10^5
ν_{max}	3.80	3.74	3.42	3.14	3.01
Γ ($kR_g = 0.1$)	15.08	13.10	8.42	6.86	6.41
Γ ($kR_g = 100$)	1.94×10^6	1.55×10^6	6.27×10^5	3.19×10^6	2.29×10^5
θ_{max}	3.66	3.63	3.42	3.19	3.06
Γ_{est}/Γ ($kR_g = 100$)	1.010	1.013	1.031	1.063	1.088

* Values of Φ and Γ are given in units of D/R_g^2

CONCLUSIONS

As N increases, $g^{(1)}(\mathbf{k}, 0)$, $g^{(2)}(\mathbf{k}, \mathbf{k}; 0)$ and the initial slope of $g^{(2)}(\mathbf{k}, \mathbf{k}; t)$ approach asymptotic forms theoretically predicted[4,29] for the long chain limits of both Rouse (free-draining) and Zimm (non-draining i.e. $h \to \infty$) models. For the Rouse model the maximum power dependence of both Φ and Γ on kR_g increases with increasing N to an asymptotic fourth power dependence predicted by de Gennes[31] (for Φ) and by Pusey[4] (for Γ), while for the Hearst approximation of the Zimm model, for $h \to \infty$, a dependence for Φ on $(kR_g)^3$ is approached, while Γ appeared to approach a dependence on $(kR_g)^{3.04}$. A third power dependence was predicted by Akcasu *et al.*[28] (for Φ) and by Pusey[4] (for Γ). The small deviation from this probably arises from imperfections in the approximations of the Hearst calculations. For both models, for large N, the dependence of Φ on kR_g was closer to its theoretical asymptotic value than that of Γ.

As $kR_g \to \infty$, both Φ and Γ vary as $(kR_g)^2$ for both Rouse and Zimm models. This was previously shown for Φ by Akcasu *et al.*[28] and was interpreted in terms of the dynamics of subunit diffusion. The value of kR_g, at which the onset of this $(kR_g)^2$-dependence was observed, increased with increasing N. Such a dependence is not, of course, predicted for Γ by the integral formula for the Rouse model (equations (21)–(23) and (30)), and clearly arises when N is finite. In addition, as kR_g increases we have found that the Gaussian factorization of $g^{(2)}$ is appropriate for large N for both Rouse and Zimm models, although the scaling law kR_g-dependence for Φ and Γ will only hold over a small range of kR_g values.

For all calculated properties of $g^{(1)}$ and $g^{(2)}$ the Hearst approximation of the Zimm model, for h varying from 0.01 to 50, gave results which varied monotonically from 'Rouse-like' at $h = 0.01$ to 'Zimm-like' (i.e. as for the $h \to \infty$ limit) at $h = 50$.

We have shown here how the asymptotic $(N \to \infty)$ theoretical predictions for the kR_g-dependence of the second and fourth order correlation functions are approached with increasing N. The dynamic correlation functions exhibit quite different N-dependence for polymer chains with and without hydrodynamic interactions. The approach of the numerical predictions to their asymptotic limits with increasing N is more rapid for the static than the dynamic correlation functions for both $g^{(1)}$ and $g^{(2)}$. All the results presented in this paper apply to the case of flexible polymers in theta solvents. The effects of excluded volume interactions on the kR_g-dependence of Γ will be treated elsewhere.

ACKNOWLEDGEMENTS

We thank User Support at the Atlas Centre, Rutherford Laboratory, for their prompt and effective assistance in running programs on the Cray X-MP/48 supercomputer. This work was supported, in part, by the Agricultural and Food Research Council of Great Britain.

REFERENCES

1 Griffin, W. G. and Pusey, P. N. *Phys. Rev. Lett.* 1979, **43**, 1100
2 Kam, Z. and Rigler, R. *Biophys. J.* 1982, **39**, 7
3 Clark, N. A., Ackerson, B. J. and Hurd, A. J. *Phys. Rev. Lett.* 1983, **50**, 1459
4 Pusey, P. N. *Macromolecules* 1985, **18**, 1950
5 Griffin, W. G., Griffin, M. C. A. and Boué, F. *Macromolecules* 1987, **20**, 2187
6 Rouse, P. E. *J. Chem. Phys.* 1953, **21**, 1272
7 Harris, R. A. and Hearst, J. E. *J. Chem. Phys.* 1966, **44**, 2595
8 Doi, M. and Edwards, S. F. 'The Theory of Polymer Dynamics', Oxford University Press, Oxford, 1986
9 Yamakawa, H. 'Modern Theory of Polymer Solutions', Harper and Row, New York, 1971
10 de Gennes, P. G. 'Scaling Concepts in Polymer Physics', Cornell University Press, Ithaca, 1979
11 Akcasu, Z. and Gurol, H. *J. Polym. Sci., Polym. Phys. Edn.* 1976, **14**, 1
12 Edwards, S. F. *Proc. Roy. Soc.* 1982, **A385**, 267
13 Baumgärtner, A. and Binder, K. *J. Chem. Phys.* 1981, **75**, 2994
14 Skolnick, J., Yaris, R. and Kolinski, A. *J. Chem. Phys.* 1988, **88**, 1407
15 Kolinski, A., Skolnick, J. and Yaris, R. *J. Chem. Phys.* 1987, **86**, 1567
16 Kolinski, A., Snolnick, J. and Yaris, R. *J. Chem. Phys.* 1987, **86**, 7164
17 Kolinski, A., Skolnick, J. and Yaris, R. *J. Chem. Phys.* 1987, **86**, 7174
18 Weill, G. and des Cloiseaux, J. *J. de Physique* 1979, **40**, 99
19 Pusey, P. N. in 'Photon Correlation Spectroscopy and Velocimetry', (Eds H. Z. Cummins and E. R. Pike) NATO ASI B23, Plenum Press, New York, 1977, p. 45
20 Berne, B. J. and Pecora, R. 'Dynamic Light Scattering with Applications to Chemistry, Biology, and Physics', Wiley, New York, 1976
21 Zimm, B. H. *J. Chem. Phys.* 1956, **24**, 269
22 Pecora, R. *J. Chem. Phys.* 1968, **49**, 1032
23 Lin, S.-C. and Schurr, J. M. *Biopolymers* 1978, **17**, 425
24 Hearst, J. E. *J. Chem. Phys.* 1962, **37**, 2547
25 Zimm, B. H., Roe, G. M. and Epstein, L. F. *J. Chem. Phys.* 1956, **24**, 279
26 Bloomfield, V. and Zimm, B. H. *J. Chem. Phys.* 1966, **44**, 315
27 Kirkwood, J. G. *J. Polym. Sci.* 1954, **12**, 1
28 Akcasu, A. Z., Benmouna, M. and Han, C. C. *Polymer* 1980, **21**, 866
29 Schaefer, D. W. and Han, C. C. 'Dynamic Light Scattering and Velocimetry: Applications of Photon Correlation Spectroscopy' (Ed. R. Pecora) Plenum Press, New York, 1985, p. 181
30 Nyquist, H. *Trans. AIEE* (Feb. 1928) pp. 617
31 de Gennes, P. G. *Physics* 1967, **3**, 37